Supplementary Information

Mechanistic Insights into CO_2 Conversion to CO Using Cyanide Manganese Complexes

Kailyn Y. Cohen, Delaan G. Nedd, Rebecca Evans, and Andrew B. Bocarsly*

Department of Chemistry, Frick Laboratory, Princeton University, Princeton, New Jersey, United States

*Email: bocarsly@princeton.edu

Contents

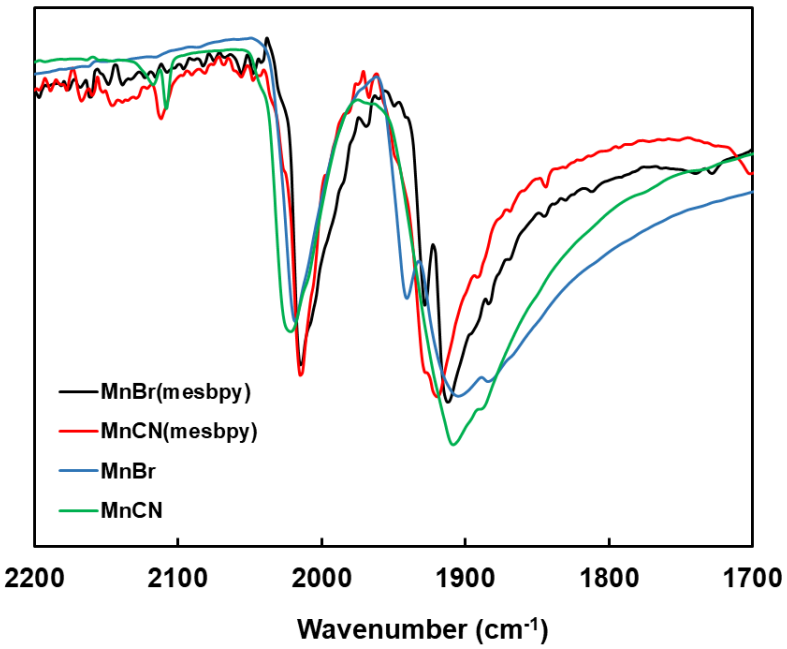

Figure S1. Solid-state ATR-IR spectra of **MnBr**, **MnCN**, **MnBr(mesbpy)**, and **MnCN(mesbpy)**. Both **MnCN** and **MnCN(mesbpy)** have terminal CN-peaks at 2115 cm^{-1}.

a)

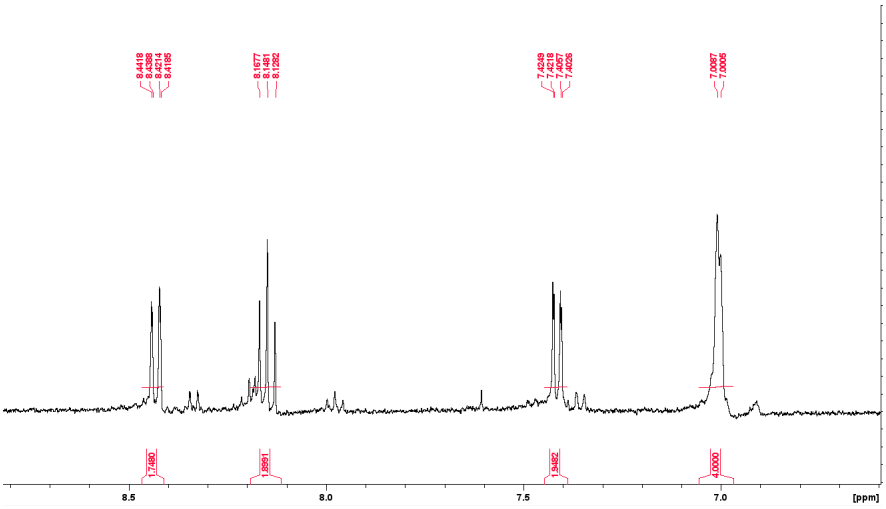

b)

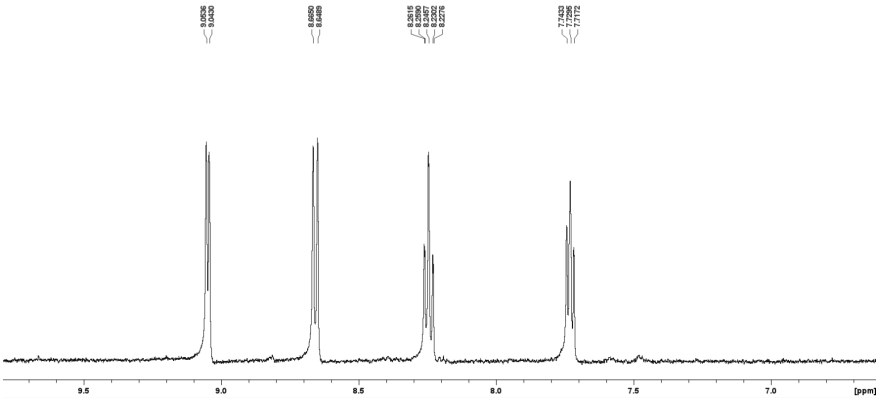

Figure S2. Aromatic region of the ^{1}H NMR of a) **MnCN(mesbpy)** in d-MeCN b) **MnCN** in DMSO-d_6.

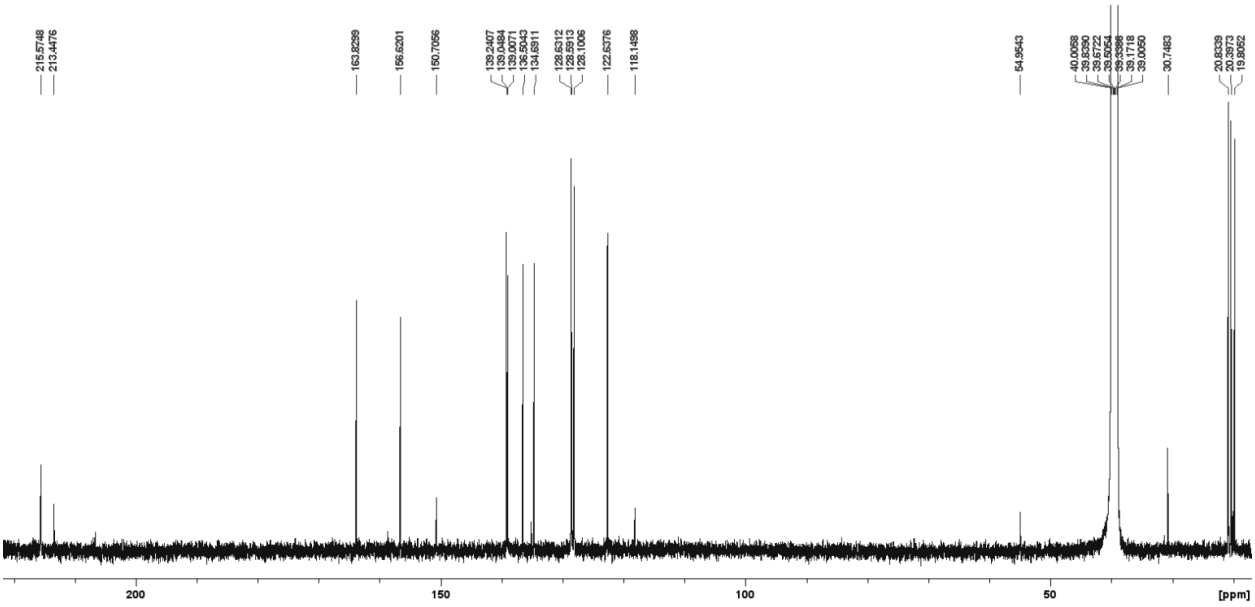

Figure S3. The carbonyl resonance region of the ^{13}C NMR spectrum in DMSO-d_6 of **MnCN(mesbpy)**, showing two carbonyl carbons at 215.5 ppm and one carbonyl carbon at 213.5 ppm. The terminal cyanide carbon is located at 163.8 ppm.

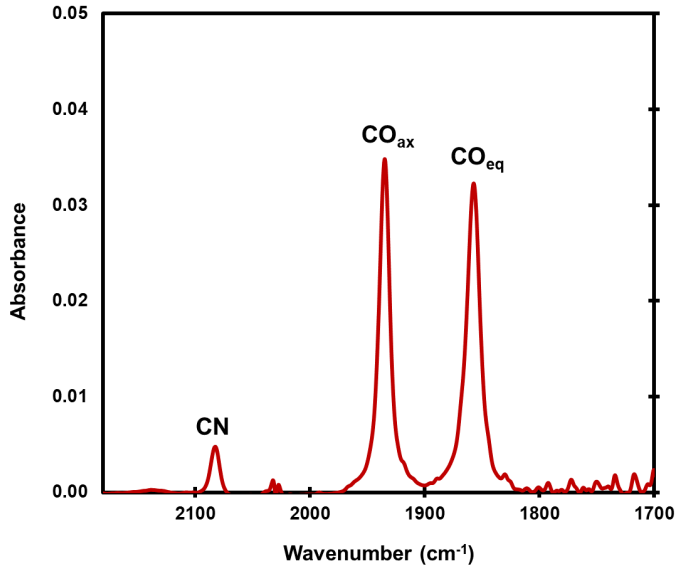

Figure S4. A difference liquid phase IR spectrum of **MnCN** after 5 s of irradiation at 395 nm, showing the formation of s-MnCN.

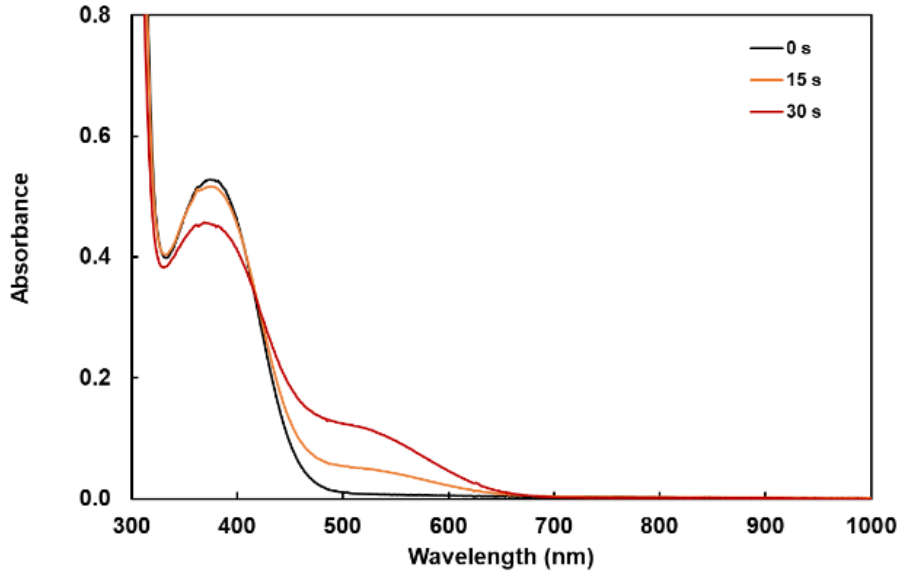

Figure S5. MnCN in MeCN under aerobic conditions before and after irradiation with a 395 nm LED (2.97×10^{-9} einstein per s intensity). The increase in the peak at ~530 nm is associated with the formation of s-MnCN, while the MLCT band of MnCN at 380 nm decreases.

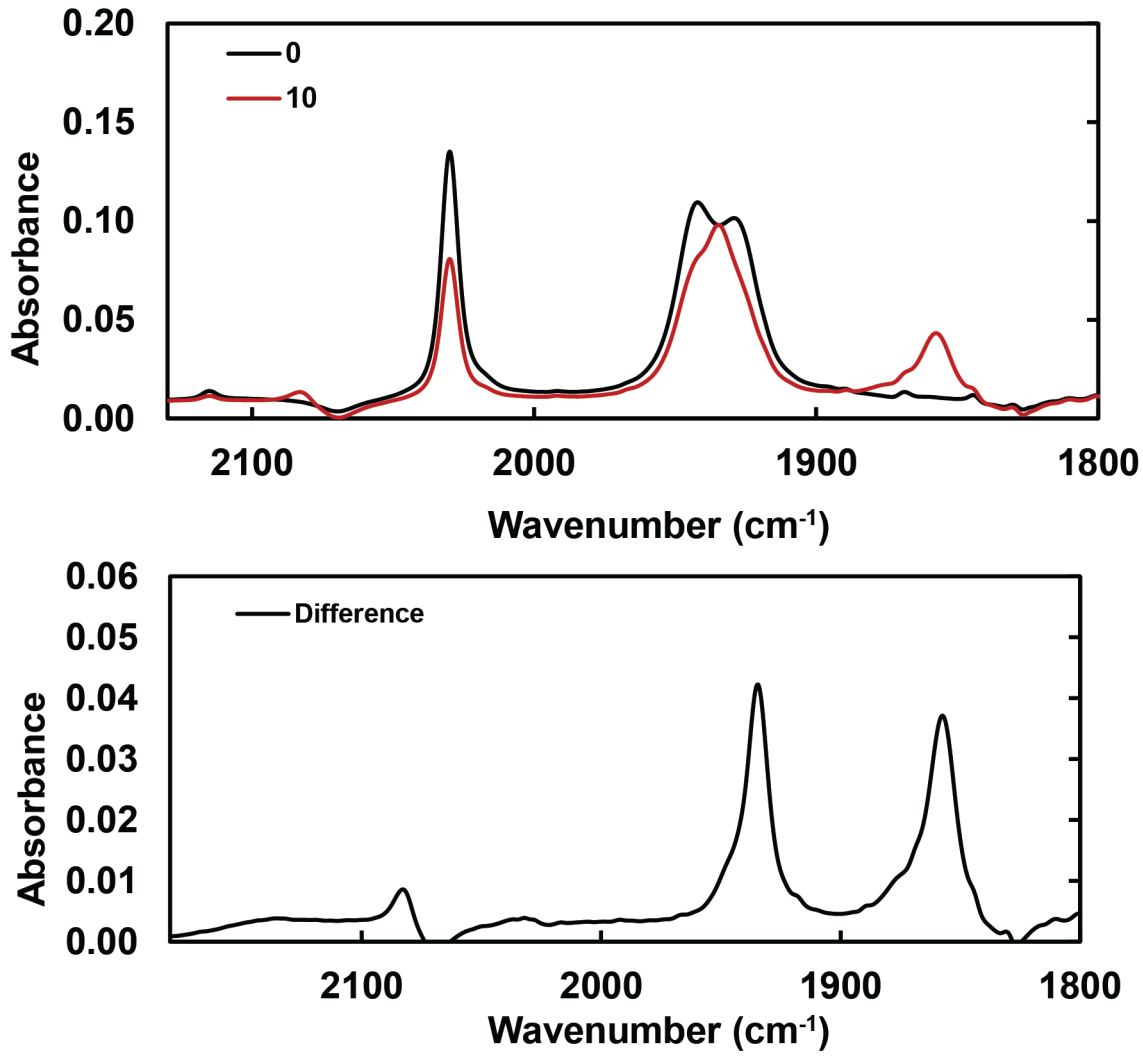

Figure S6. Liquid phase IR of a 10:1 mixture of **MnCN** and PPh_3 in dry, degassed MeCN after 10 s of irradiation at 395 nm showing retention of the terminal cyanide ligand. ^{31}P NMR (below) shows PPh_3 ligation to the Mn center.

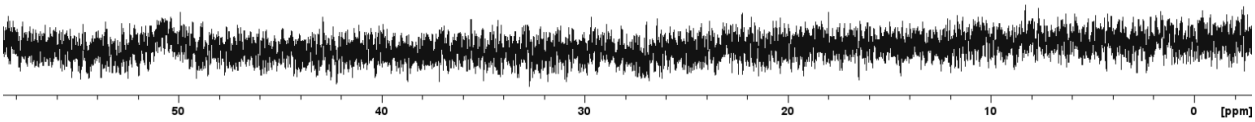

Figure S7. ^{31}P NMR showing PPh_3 ligation. The NMR sample was prepared by irradiating a 10:1 mixture of MnCN and PPh_3 in dry, degassed d-MeCN for 10 s at 395 nm. Liquid IR (above) confirms retention of the terminal CN ligand. ^{31}P NMR spectra were referenced to 85% H_3PO_4 solution as an external standard in d-MeCN.

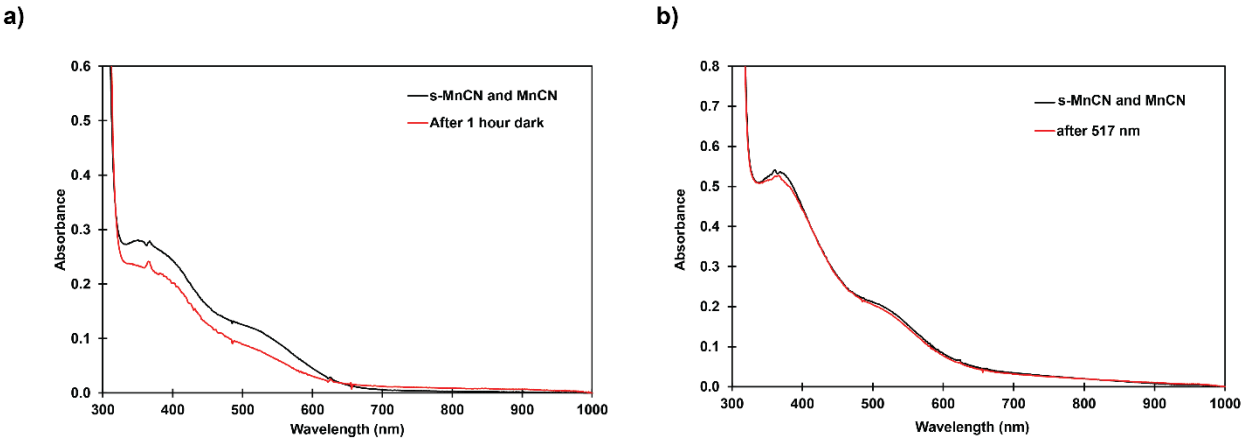

Figure S8. UV-vis spectra of a) a mixture of **s-MnCN** and **MnCN** before (black) and after (red) sitting in the dark over the course of 1 hour and b) a mixture of **s-MnCN** and **MnCN** before (black) and after (red) irradiation at 517 nm for 60 s in dry, degassed MeCN.

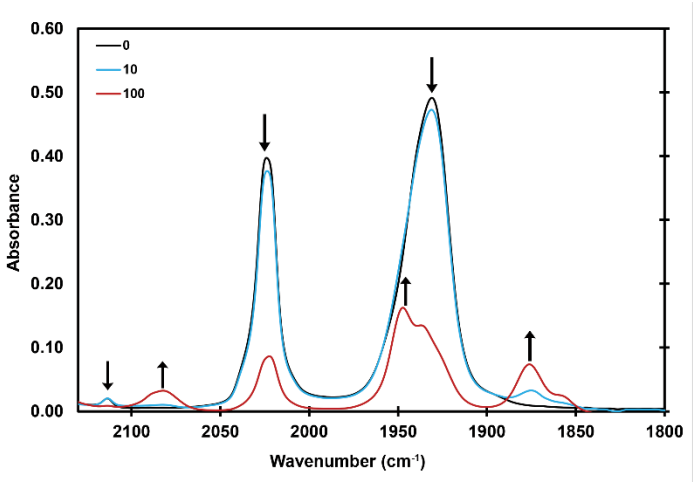

Figure S9. Liquid phase IR spectra of **MnCN(mesbpy)** after 100 s of 395 nm irradiation. The terminal cyanide peak at 2081 cm^{-1} and the two carbonyl peaks at 1949 and 1873 cm^{-1} indicate formation of **s-MnCN(mesbpy)**,[1] where one equatorial CO is replaced by a MeCN solvent ligand.

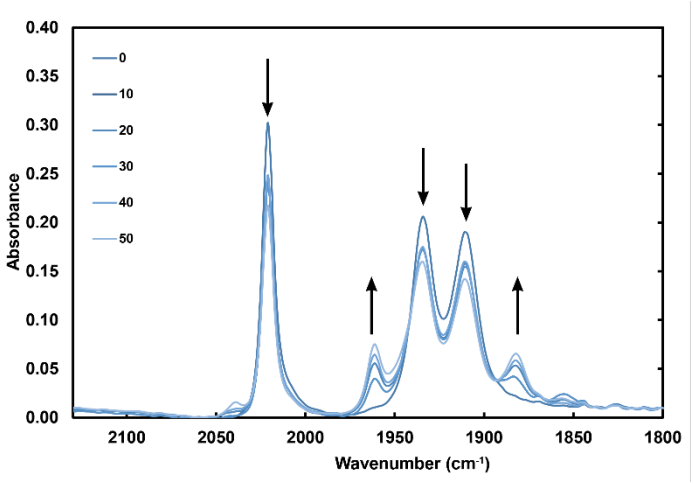

Figure S10. Liquid phase IR spectra of MnBr(mesbpy) after 50 s of 395 nm irradiation. The two carbonyl peaks at 1961 and 1882 cm^{-1} indicate formation of a bis-acetonitrile species,[1] $[Mn(mesbpy)(CO)_2(MeCN)_2]^+$ where the Br ligand and an equatorial CO are replaced by MeCN solvent ligands. The small peak at 2038 cm^{-1} is assigned to *mer*-MnBr(mesbpy).

Nicholson and Shain Diagnostics

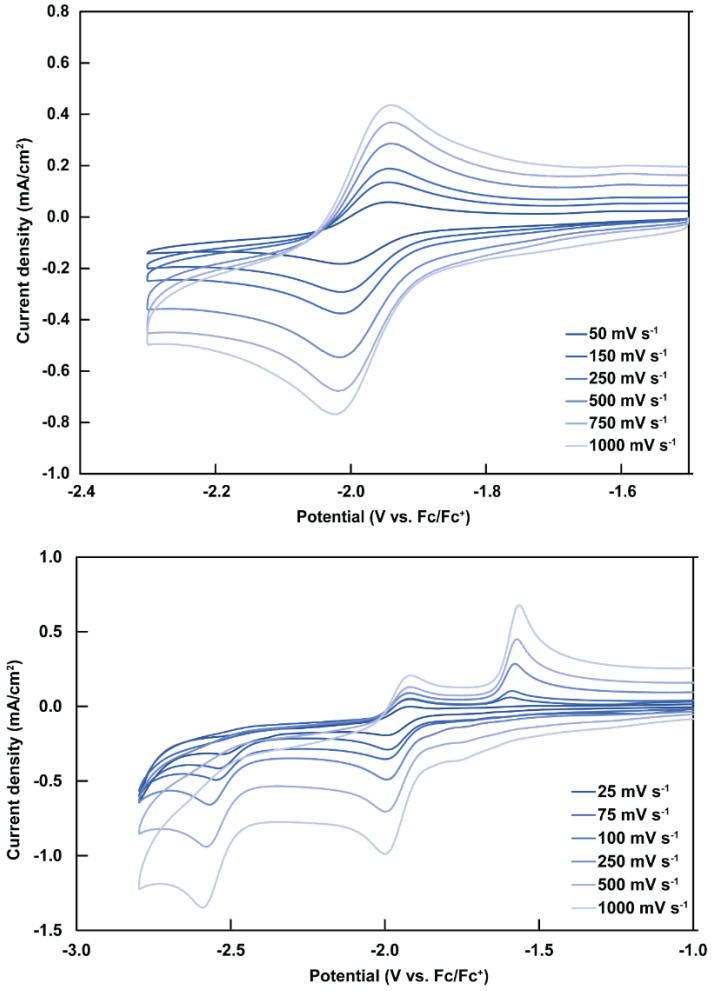

Figure S11. Cyclic voltammetry of [Mn(mesbpy)$(CO)_3$CN] (1 mM) under Ar in dry MeCN with 0.1 M $TBAPF_6$ supporting electrolyte. The switching potentials were set to −2.3 V vs Fc/Fc^+ (top) and −2.9 V vs Fc/Fc^+ (bottom).

Nicholson and Shain diagnostics were performed for all four peaks, revealing that the first reduction and first oxidation events are reversible, while all four features are diffusion-limited (**Figure S12-14**)

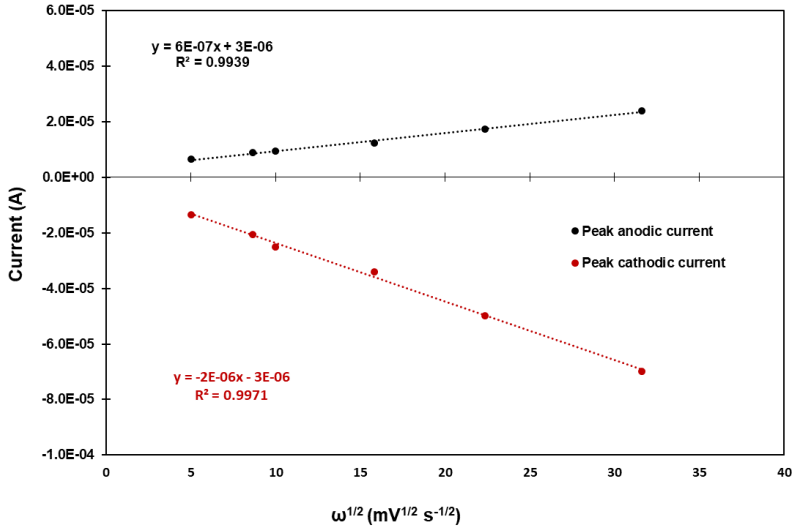
y = 6E-07x + 3E-06
R² = 0.9939
y = -2E-06x - 3E-06
R² = 0.9971
Peak anodic current
Peak cathodic current
Current (A)
ω^1/2 (mV^1/2 s^-1/2)

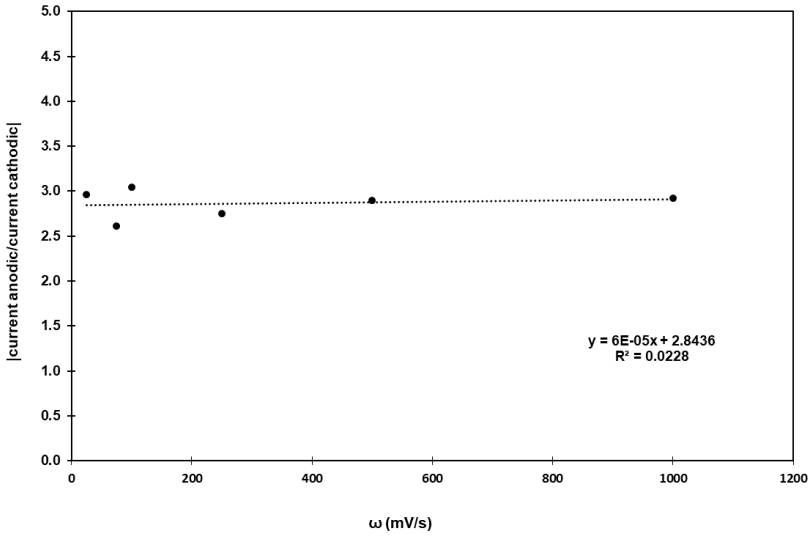
y = 6E-05x + 2.8436
R² = 0.0228
|current anodic/current cathodic|
ω (mV/s)

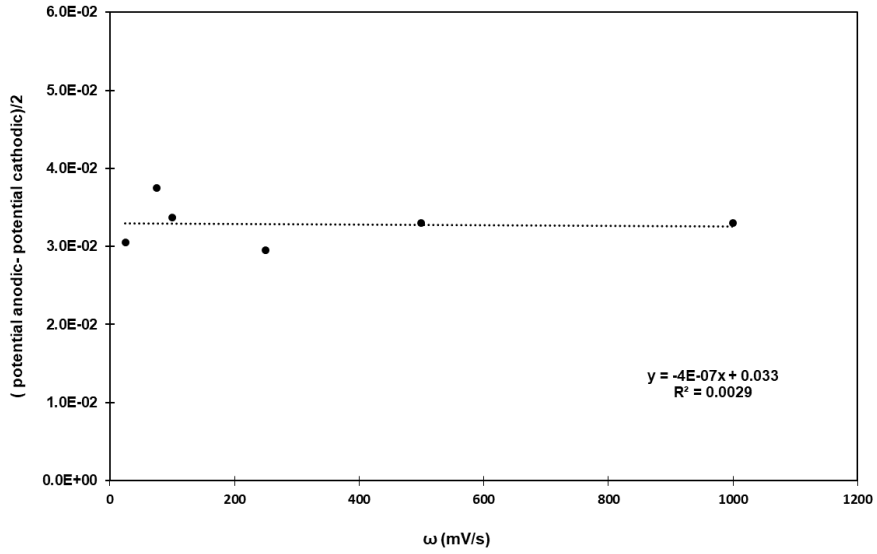

Figure S12. Nicholson and Shain Diagnostics for **MnCN(mesbpy)** for the first reduction peak at -1.98 V and the first oxidation peak at -1.91 V vs. Fc/Fc^{+}.

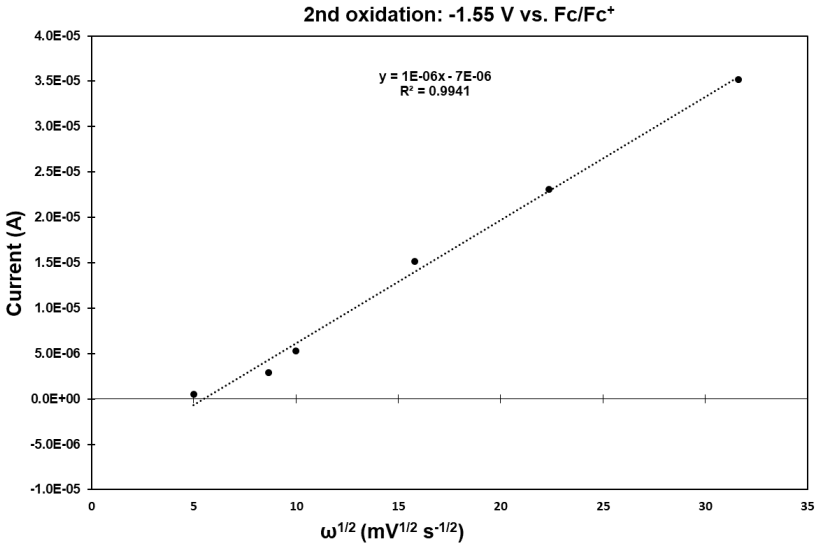

Figure S13. Current vs. $(\text{scan rate})^{1/2}$ for **MnCN(mesbpy)** for the second oxidation peak at -1.55 V vs. Fc/Fc^{+}.

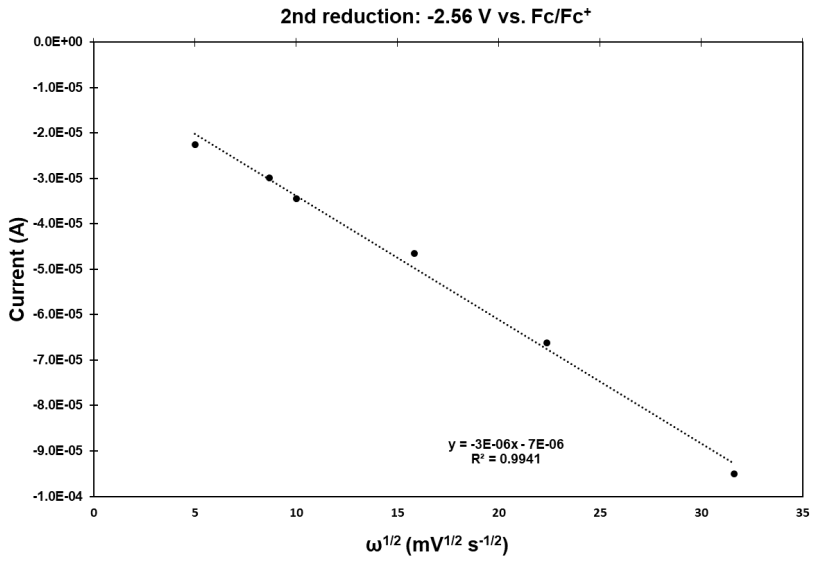

Figure S14. Current vs. (scan rate)$^{1/2}$ for **MnCN(mesbpy)** for the second reduction peak at -2.56 V vs. Fc/Fc^{+}.

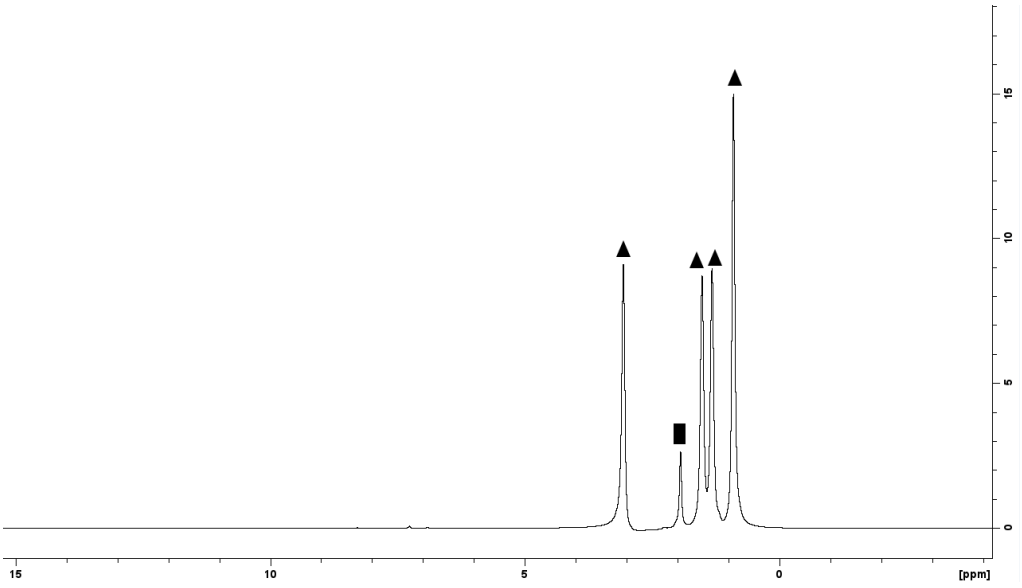

Figure S15. A sample ^{1}H NMR spectrum in $CDCl_3$ of 4-hour bulk electrolysis run at the second reduction potential of **MnCN(mesbpy)** using 5% v/v H_2O as the proton source**.** The MeCN solvent was mostly removed in vacuo, but is indicated with a ▮, while the $TBAPF_6$ supporting electrolyte is indicated by ▲. No formic acid is observed, which would have signals appearing at 10.99 and 8.06 ppm.

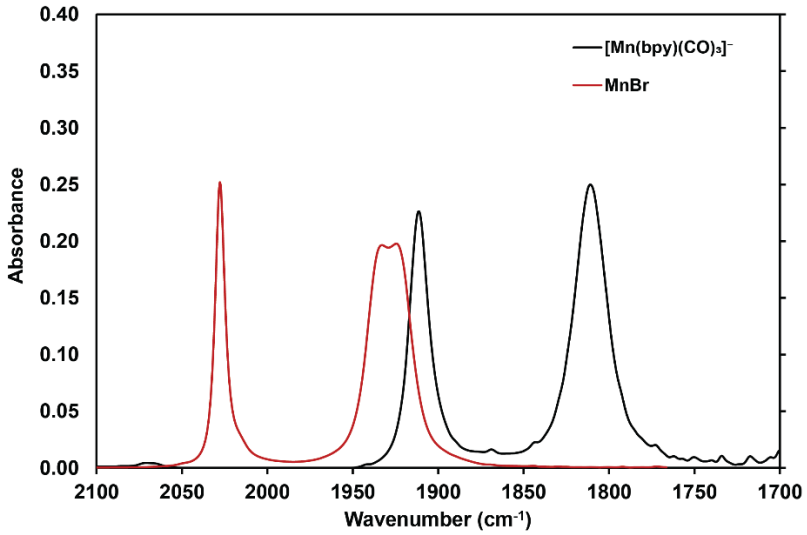

Figure S16. Liquid phase IR spectra of a pristine sample of **MnBr** and $[Mn(bpy)(CO)_3]^-$ in dry, degassed MeCN. $[Mn(bpy)(CO)_3]^-$ was synthesized by added two equivalents of Na(Hg) to a sample of **MnBr** in MeCN.

Example Quantum Yield Calculation:

$$Quantum\ Yield = \left(mol\ CO \Big/ \frac{(light\ absorbed, W)(irradiation\ time, s)}{(energy\ per\ Einstein)} \right)$$

$$0.51 = \left(30.45\ x\ 10^{-6}\ mol\ CO \Big/ \frac{(0.00504\ J/s)(3600\ s)}{\left(\frac{hc}{395\ x\ 10^{-9}\ m}\right) N_A} \right)$$

$$Corrected\ Quantum\ Yield = Quantum\ Yield \times 6.1\%$$

$$0.031 = 0.51 \times 6.1\%$$

Intensity absorbed = 5.04 mW @ 395 nm

Energy per Einstein = (hc/395 E -9 m)*N_A where N_A = Avogadro's number

Irradiation time = 3600 s

X-ray Crystallography

A single crystal suitable for X-ray diffraction analysis of **MnCN(mesbpy)** was isolated by layering diethyl ether over a dichloromethane solution at 298 K, resulting in a translucent pale orange crystal. Single X-ray diffraction data were collected using a Bruker Apex Duo CCD detector using MoKα radiation. SADABS V2014/2 (Bruker AXS Inc.) was used to perform absorption corrections. The frames were integrated with the Bruker SAINT V8.34A software package.

Collection Data for **MnCN(mesbpy)**
Formula: $C_{32}H_{28}MnN_3O_3$
Formula Weight: 557.51
Crystal System: monoclinic
Space Group: C 2/c

Unit Cell Dimensions:

a = 35.058(4) Å
b = 8.1500(9) Å
c = 23.637(3) Å
alpha = 90 degrees
beta = 115.810(4) degrees
gamma = 90 degrees

Cell Volume: 6079.9 $Å^3$
Temperature: 100 K
Radiation Type: MoKα
Radiation Wavelength: 0.71073 Å
Theta range for data collection: 1.290 degrees to 29.566 degrees
Reflections Collected: 71338
Goodness-of-fit on F^2: 1.033

Bond Lengths (Å):
Mn1-N2, 2.099(2)
Mn1-C37, 1.804(3)
Mn1-C35, 1.803(3)
Mn1-C33, 1.832(2)
Mn1-C31, 2.003(2)
Mn1-N7, 2.087(2)
N2-C3, 1.347(4)
N2-C16, 1.358(3)
C3-C4, 1.486(3)
C3-C13, 1.397(4)
C4-C5, 1.396(3)
C4-C11, 1.400(3)
C5-C6, 1.512(3)

C5-C7, 1.392(4)
C6-H6A, 0.982
C6-H6B, 0.979
C6-H6C, 0.981
O38-C37, 1.150(4)
O36-C35, 1.143(3)
O34-C33, 1.143(3)
N32-C31, 1.150(3)
C7-H7, 0.95
C7-C8, 1.393(3)
N7-C17, 1.371(4)
N7-C21, 1.342(4)
C8-C9, 1.503(4)
C8-C10, 1.379(4)
C9-H9A, 0.98
C9-H9B, 0.98
C9-H9C, 0.98
C10-H10, 0.95
C10-C11, 1.386(4)
C11-C12, 1.511(4)
C12-H12A, 0.98
C12-H12B, 0.981
C12-H12C, 0.979
C13-H13, 0.95
C13-C14, 1.367(4)
C14-H14, 0.951
C14-C15, 1.367(5)
C15-H15, 0.95
C15-C16, 1.405(4)
C16-C17, 1.451(5)
C17-C18, 1.392(3)
C18-H18, 0.95
C18-C19, 1.367(5)
C19-H19, 0.95
C19-C20, 1.374(5)
C20-H20, 0.95
C20-C21, 1.401(4)
C21-C22, 1.497(4)
C22-C23, 1.401(4)
C22-C29, 1.391(3)
C23-C24, 1.507(3)
C23-C25, 1.379(4)
C24-H24A, 0.981
C24-H24B, 0.979
C24-H24C, 0.98
C25-H25, 0.95

C25-C26, 1.398(3)
C26-C27, 1.498(5)
C26-C28, 1.384(5)
C27-H27A, 0.979
C27-H27B, 0.98
C27-H27C, 0.98
C28-H28, 0.95
C28-C29, 1.393(4)
C29-C30, 1.508(5)
C30-H30A, 0.98
C30-H30B, 0.979
C30-H30C, 0.98

Bond Angles (degrees):

N2	Mn1	C37	174.3(1)
N2	Mn1	C35	98.6(1)
N2	Mn1	C33	97.8(1)
N2	Mn1	C31	84.60(9)
N2	Mn1	N7	78.49(8)
C37	Mn1	C35	81.2(1)
C37	Mn1	C33	87.9(1)
C37	Mn1	C31	89.8(1)
C37	Mn1	N7	101.0(1)
C35	Mn1	C33	91.3(1)
C35	Mn1	C31	87.8(1)
C35	Mn1	N7	172.4(1)
C33	Mn1	C31	177.5(1)
C33	Mn1	N7	96.1(1)
C31	Mn1	N7	84.9(1)
Mn1	N2	C3	129.0(2)
Mn1	N2	C16	112.2(2)
C3	N2	C16	117.4(2)
N2	C3	C4	121.0(2)
N2	C3	C13	122.2(2)
C4	C3	C13	116.8(2)
C3	C4	C5	119.0(2)
C3	C4	C11	119.6(2)
C5	C4	C11	120.8(2)
C4	C5	C6	121.4(2)
C4	C5	C7	118.7(2)
C6	C5	C7	119.8(2)
C5	C6	H6A	109.4
C5	C6	H6B	109.5
C5	C6	H6C	109.5

H6A	C6	H6B	109.5
H6A	C6	H6C	109.5
H6B	C6	H6C	109.5
Mn1	C37	O38	170.4(2)
Mn1	C35	O36	171.7(2)
Mn1	C33	O34	173.2(2)
Mn1	C31	N32	178.7(2)
C5	C7	H7	119.3
C5	C7	C8	121.5(2)
H7	C7	C8	119.3
Mn1	N7	C17	112.8(2)
Mn1	N7	C21	129.0(2)
C17	N7	C21	117.8(2)
C7	C8	C9	120.7(3)
C7	C8	C10	118.3(3)
C9	C8	C10	121.0(3)
C8	C9	H9A	109.5
C8	C9	H9B	109.5
C8	C9	H9C	109.5
H9A	C9	H9B	109.4
H9A	C9	H9C	109.5
H9B	C9	H9C	109.4
C8	C10	H10	118.8
C8	C10	C11	122.4(3)
H10	C10	C11	118.8
C4	C11	C10	118.3(2)
C4	C11	C12	120.7(2)
C10	C11	C12	121.0(3)
C11	C12	H12A	109.4
C11	C12	H12B	109.5
C11	C12	H12C	109.4
H12A	C12	H12B	109.5
H12A	C12	H12C	109.4
H12B	C12	H12C	109.5
C3	C13	H13	120.1
C3	C13	C14	119.9(3)
H13	C13	C14	120
C13	C14	H14	120.6
C13	C14	C15	118.7(3)
H14	C14	C15	120.7
C14	C15	H15	120.2
C14	C15	C16	119.6(3)
H15	C15	C16	120.2
N2	C16	C15	121.8(2)
N2	C16	C17	115.9(2)

C15	C16	C17	122.3(2)
N7	C17	C16	116.1(2)
N7	C17	C18	122.6(2)
C16	C17	C18	121.4(2)
C17	C18	H18	120.5
C17	C18	C19	118.9(3)
H18	C18	C19	120.6
C18	C19	H19	120.5
C18	C19	C20	119.1(3)
H19	C19	C20	120.4
C19	C20	H20	119.8
C19	C20	C21	120.3(3)
H20	C20	C21	119.9
N7	C21	C20	121.3(3)
N7	C21	C22	121.0(2)
C20	C21	C22	117.7(2)
C21	C22	C23	117.8(2)
C21	C22	C29	121.1(2)
C23	C22	C29	120.8(2)
C22	C23	C24	121.3(2)
C22	C23	C25	118.8(2)
C24	C23	C25	119.9(3)
C23	C24	H24A	109.5
C23	C24	H24B	109.5
C23	C24	H24C	109.4
H24A	C24	H24B	109.4
H24A	C24	H24C	109.4
H24B	C24	H24C	109.5
C23	C25	H25	119
C23	C25	C26	121.9(3)
H25	C25	C26	119
C25	C26	C27	120.4(3)
C25	C26	C28	117.8(3)
C27	C26	C28	121.9(3)
C26	C27	H27A	109.4
C26	C27	H27B	109.4
C26	C27	H27C	109.5
H27A	C27	H27B	109.5
H27A	C27	H27C	109.5
H27B	C27	H27C	109.5
C26	C28	H28	119
C26	C28	C29	122.1(3)
H28	C28	C29	118.9
C22	C29	C28	118.5(3)
C22	C29	C30	121.6(3)

C28	C29	C30	119.7(3)
C29	C30	H30A	109.5
C29	C30	H30B	109.5
C29	C30	H30C	109.5
H30A	C30	H30B	109.4
H30A	C30	H30C	109.5
H30B	C30	H30C	109.4

1. Yempally, V.; Moncho, S.; Hasanayn, F.; Fan, W. Y.; Brothers, E. N.; Bengali, A. A., Ancillary Ligand Effects upon the Photochemistry of Mn(bpy)$(CO)_3$X Complexes (X = Br^- , $PhCC^-$). *Inorganic Chemistry* **2017,** *56* (18), 11244-11253.